Received: 13 December 2017 | Revised: 16 February 2018 | Accepted: 3 July 2018

DOI: 10.1002/nag.2849

RESEARCH ARTICLE

WILEY

Fracture behavior of transversely isotropic rocks with discrete weak interfaces

Humberto M. Celleri[1,2,3] | Martín Sánchez[1] | José L. Otegui[1,3]

[1]YPF-Tecnología S.A. (Y-TEC), Geosciences department, Berisso 1923, Argentina

[2]Facultad Regional La Plata, Universidad Tecnológica Nacional, La Plata 1900, Argentina

[3]Consejo Nacional de Investigaciones Científicas y Técnicas (CONICET), Ciudad Autónoma de Buenos Aires 1425, Argentina

Correspondence
Martín Sánchez, YPF-Tecnología S.A. (Y-TEC), Av del Petróleo S/N, Berisso 1923, Argentina.
Email: martin.sanchez@ypftecnologia.com

Summary

Anisotropic rocks have gained increasing attention due to the development of unconventional oil and gas reservoirs. This type of reservoir requires complex engineering procedures from drilling to completion, and the mechanical properties of the rocks play a significant role. One of the most important characteristics of unconventional formations is the presence of well-defined layers, which greatly modify both elastic and fracture properties of the rocks. Rock elastic response is direction dependent, commonly described as vertically transversely isotropic (VTI), meaning that there is an isotropic plane of symmetry with respect to the vertical direction. Between layers, calcitic veins or ash beds alter the rock's properties substantially. These interfaces, which can have low or no cohesion at all, act as preferential planes for fracture nucleation and propagation, affecting the rocks strength. In this work, the fracture behavior of VTI rocks with weak interfaces is studied using numerical simulations of brazilian tests. A hybrid discontinuous Galerkin–cohesive zone model was used to simulate fracture initiation and propagation on discs in the presence of weak planes. With this approach, we determined the effective brazilian test strength of the rocks under different conditions, namely, relative angles between layers and the loading direction, densities, and cohesion of weak interfaces. Shear reactivation of the interfaces is analyzed using the Mohr-Coulomb failure criterion and Mohr circles.

KEYWORDS

anisotropic rocks, Brazilian test, numerical simulations, vertically transversely isotropic, weak interfaces

1 | INTRODUCTION

Many sedimentary and metamorphic rocks present well-defined fabric such as foliation, lamination, or stratification, as a consequence of their deposition and diagenetic history. The fabric, which generates direction-dependent mechanical properties, is present in the form of mineralogical alignment or fine laminations.

A particular group of anisotropic rocks consist of those which have a plane of isotropy perpendicular to the direction of sedimentological deposition. This type of behavior is known as vertically transversely isotropic (VTI).[1] Metamorphic rocks with foliation (eg, slate and gneiss) and laminated sedimentary rocks (eg, shale), among many others, are considered VTI rocks.

Anisotropic rocks can be also heterogeneous at different scales. Many of these rocks present well-defined weak interfaces in the form of calcitic veins or ash beds acting as preferential spots for fracture nucleation and propagation. Fracture properties on these interfaces can differ significantly from those of the anisotropic matrix, having lower or even no cohesion at all. This type of rocks has gained interest because of the increasing production of shale oil and gas reservoirs. The economic development of these formations depends on an effective hydraulic fracture stimulation process of the reservoir, which is largely affected by the rock's mechanical properties. The study of fracture initiation and propagation in this anisotropic medium with weak interfaces is essential to understand and optimize the well completion in unconventional reservoirs.

The tensile strength is one of the most important parameters to characterize the fracture process of rocks. Many indirect tests have been suggested to measure fracture parameters of rocks: the bending cylinder test,[2] the semicircular bending disc test,[3] and the brazilian disc test,[4] among many others. Generally, these tests are used to study the tensile behavior of isotropic materials indirectly.[5]

The brazilian test (BT) is a well-known indirect method for determining rock tensile strength. The method has been applied extensively in rock engineering because specimens can be easily prepared, and the test is simple to perform. Many experimental studies have used the BT to characterize the strength of VTI rocks. There is a general consensus about the effect that weak layers have in anisotropic rocks; layers make the rock's behavior dependent on the angle of loading. Vervoort et al[6] performed a series of experimental tests on nine different types of anisotropic rocks. They analyzed the influence of the orientation angle of the weak plane on the final strength and failure. Their results showed the complexity of the fracture behavior of such rocks, which was summarized by assuming four different trends depending on the degree of anisotropy.

Debecker and Vervoort[7] studied a layered slate under different test conditions. They found that the strength in the direction of the schistosity (direction of the layers) is considerably less than in the other directions. Their work also suggested that a key factor of that behavior could be strength's anisotropy on the microscale. Tavallali and Vervoort[9] analyzed the effect of microparameters on the fracture process of layered sandstones. They found that both the number and the spacing between planes affect the fracture pattern and introduced the concept of percentage of fracture propagating in the weak plane direction as a way to characterize the percentage of weak plane sliding.

Tan et al[10] performed a series of BT on Mosel slate considering different foliation-loading angles. Fracture patterns and strength of samples were analyzed, and the deformation process and failure behavior were simulated using the discrete element method (DEM). They found tensile fracture mode for low and high angles and mixed modes for intermediate angles. A schematic diagram of failure modes distribution was introduced. This type of diagram helps to identify failure mode zones, depending on either the rock's properties or the load-weak plane's orientation angle. Khanlari et al[11] used the isotropic ISRM BT expression[5] to obtain the brazilian tensile strength (BTS) on laminated sandstones. Varying the load angle, they analyzed the percentage of fracture on the weak direction or in the matrix. They found an important variation of the BTS only for high loading angle (greater than 60°). Mighani et al[12] characterized two anisotropic groups of rocks using a micro-CT scan and SEM images. Fracture behavior was analyzed using BT. For conventional anisotropic (mineralogical alignment) sandstones, they found a 60% decrease in BTS. On the other hand, anisotropic veining (calcitic-filled) profoundly reduces the BTS, almost by a factor of two.

Foliation not only affects the fracture properties of rocks but also generates anisotropy in the elastic response. A VTI material requires five elastic constants to fully characterize the elastic behavior. Amadei et al[13] introduced a solution to obtain the stresses in an anisotropic disc under diametrically opposite loads. Additionally, Chen et al[14] used Amadei's analytical solution to present BT stress distribution diagrams of transversely isotropic materials. Claesson and Bohloli[15] continued the work of Chen et al[14] and introduced an approximate expression for the tensile stress state at the center of a brazilian VTI disc with a semiarc load.

Cho et al[16] experimentally obtained the VTI elastic properties of Asan gneiss, Boryeong shale, and Yeoncheon schist. They used Claesson-Bohloli[15] approximate expression to obtain the stress state at the center of the brazilian disc. For some of the most anisotropic rocks they studied, the error associated with using Claesson-Bohloli solution is greater than 10%, and this error seems not to have been taken into account.

In order to be valid, BT fracture initiation should be at the center of the disc. Kourkoulis et al[17] studied the contact problem associated with load application to a circular disc. They obtained a well-correlated solution between their model and experimental results. Erarslan and Williams[18] analyzed experimentally and numerically the loading contact problem associated with the BT of Brisbane tuff. It was concluded that BTS is strongly dependent on the type of diametrical loading. They show that a 30° loading arc resulted in the most central-located diametrical splitting fractures.

Many numerical methods have been developed to simulate fracture initiation and propagation. The DEM was used to simulate schistosity planes in slates.[10,19] The strength anisotropy was obtained using an isotropic material model with discontinuities. Yang et al[20] used DEM to model the brazilian splitting test for jointed rock mass specimens. These joints produce different modes of fracture, depending on the angle of loading. Bonded-particle DEM with embedded smooth joints was used by Park and Min[21] to simulate the mechanical behavior of VTI rocks. The cohesion of weak interface is found to have an important effect on the final tensile strength. Duan et al[22] used DEM simulations with different degrees of anisotropy to reproduce the four trends analyzed by Vervoort et al.[6] They found that the friction angle has a minor effect on the mechanical behavior. Mahabadi et al[23] used a hybrid FEM-DEM method to simulate failure processes. The rock fabric was reproduced using a CT scan and digital techniques to study the grain heterogeneity distribution in the sample.

Heterogeneous fracture behavior can be due to mineralogical alignment or to preferential paths that promote the crack growth (eg, natural fractures and weak interfaces). Most of the numerical models used to analyze the BT take into account only the fracture anisotropic behavior with the inclusion of planes with different cohesion and internal friction embedded in an isotropic matrix (see, for example, references herein[19,21,24]). However, numerical investigation of fracture initiation and propagation in this type of rocks requires the application of more complex material models in order to correctly reproduce the elastic and the fracture behaviors together.

Mahjoub et al[25] used a fictitious isotropic material to represent the stress state in VTI rocks. They extended a Drucker-Prager failure criterion for this fictitious isotropic formulation and studied the strength dependence with the orientation angle in brazilian tests. They found that for highly anisotropic rocks, the proposed model lacked the ability to reproduce the proposed results.

Most of the works in this field have studied the fracture behavior of rocks considering an isotropic rock matrix with separate weak interfaces,[10,19] or taking into account an anisotropic matrix in which the foliation effect is included as a whole.[22] However, the presence of weak interfaces with different degree of cohesion can alter the fracture behavior of an intrinsically anisotropic rock. The effect of discrete weak interfaces on the fracture behavior of VTI rocks is an ongoing field of research.

In this article, the effect of weak interfaces embedded on an anisotropic-VTI matrix is numerically modeled to characterize the fracture process in brittle rocks. Numerical modeling of BT under opposite plane jaws is analyzed using a hybrid discontinuous Galerkin (DG)–cohesive zone model (CZM). With this approach, we determined the effective brazilian test strength of the rocks under different conditions, namely, relative angles between layers and the loading direction, densities, and cohesion of weak interfaces. Fracture initiation, propagation, and interfaces reactivation are explained based on a modified matrix-weak interface Mohr-Coulomb criterion.

2 | BRAZILIAN TEST

The BT is a standard mechanical test that has been used to indirectly measure the tensile strength of rocks using cylindrical discs. During a BT, a diametral compression load is applied; because of this compression, a tensile stress state develops at the disc center.

We show in Figure 1 a schematic diagram of the BT of a VTI rock with weak interfaces. A recent review[26] described the analytical, numerical, and experimental state-of-the-art of the use of the BT to characterize rocks' mechanical properties. While isotropic rocks have been widely studied, the principal characteristics of anisotropic rocks are subject of current research.

A solution to obtain the stress distribution in a VTI brazilian disc test was developed by considering homogeneous anisotropic rocks, leaving aside the intrinsic heterogeneous characteristics of weak interfaces.[13] This may over simplify the elastic and fracture response of some VTI rocks, where the effects of anisotropy can be important. However, it is a regular practice to use the ultimate load of the BT to estimate the tensile strength of the sample.[5]

For isotropic rocks, the tensile strength can be estimated using the expression given by[27]

$$\sigma_t = \frac{2P}{\pi D t}, \tag{1}$$

where P is the BT's ultimate load, D and t are the sample's diameter and width.

As we mentioned before, Equation 1 is only valid when a uniform tensile stress state in the middle of the disc is generated, and the fracture process does not initiate near to the loading application point. Recently, Claesson and Bohloli obtained an approximate expression (Equation 2) for the tensile stress state (σ_t) in the center of a BT specimen for anisotropic rocks[15]:

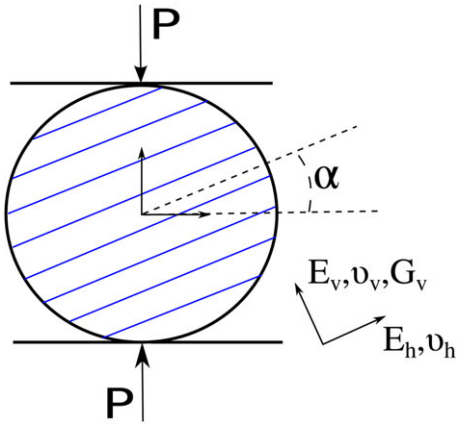

FIGURE 1 Vertically transversely isotropic rock under diametrically opposite loads P. The blue lines inside the disc specimen correspond to the weak interfaces at an angle α with respect to the horizontal direction. E_h, ν_h and E_v, ν_v are the Young moduli and Poisson ratios of the rock in the horizontal and vertical directions respectively [Colour figure can be viewed at wileyonlinelibrary.com]

$$\sigma_t \cong \frac{2P}{\pi Dt}\left[\sqrt[4]{\frac{E_h}{E_v}}^{\cos(2\alpha)} - \frac{\cos(4\alpha)}{4}(b-1)\right], \tag{2}$$

where

$$b = \frac{\sqrt{E_h E_v}}{2}\left(\frac{1}{G_v} - \frac{2\nu_v}{E_v}\right). \tag{3}$$

E_h, ν_h and E_v, ν_v are the Young moduli and Poisson ratios of the rock in the horizontal and vertical directions, respectively, and G_v is the shear modulus.

3 | NUMERICAL METHODS AND SIMULATION MODEL

3.1 | Anisotropic rock material model

The mechanical properties of many sedimentary and metamorphic rocks depend on the direction of the applied load.

The VTI materials require five independent elastic constants to fully characterize their elastic response. The stiffness tensor $\boldsymbol{C}$, in Voigt notation for the VTI model, is defined by Equation 4:

$$\boldsymbol{C} = \begin{pmatrix} C_{11} & C_{12} & C_{13} & 0 & 0 & 0 \\ C_{12} & C_{11} & C_{13} & 0 & 0 & 0 \\ C_{13} & C_{13} & C_{33} & 0 & 0 & 0 \\ 0 & 0 & 0 & C_{44} & 0 & 0 \\ 0 & 0 & 0 & 0 & C_{44} & 0 \\ 0 & 0 & 0 & 0 & 0 & \frac{1}{2}(C_{11} - C_{12}) \end{pmatrix}, \tag{4}$$

where C_{ij} are the elastic components of the stiffness tensor.

Transversely isotropic elastic constants (Equation 4) can be obtained from the engineering elastic parameters. It can be shown that the stiffness constants are given by Suarez-Rivera et al[28]:

$$\begin{aligned} C_{11} &= E_h(1 - \frac{E_h}{E_v}\nu_v^2)/A \\ C_{33} &= E_v(1 - \nu_h^2)/A \\ C_{44} &= 2G_v \\ C_{13} &= E_h\nu_v(\nu_h + 1)/A \\ C_{12} &= E_h(\frac{E_h}{E_v}\nu_v^2 + \nu_h)/A \end{aligned} \tag{5}$$

with

$$A = (1 + \nu_h)(1 - 2\frac{E_h}{E_v}\nu_v^2 - \nu_h). \tag{6}$$

Once the stiffness tensor is defined, it is necessary to rotate it from the local coordinate system where one axis has the direction of the weak planes, to a global one where the loading direction is one of the principal axis. The material stiffness tensor **C** can be transformed using Bond matrix $\mathbf{R}^1$ from the local to a global configuration **C'**:

$$\boldsymbol{C}' = \mathbf{R}\boldsymbol{C}\mathbf{R}', \tag{7}$$

where **R'** is the transposed matrix of **R**.

The implemented VTI model not only has direction-dependent elastic properties but also allows to use well-defined interface properties. This interface's properties can vary independently from those of the anisotropic matrix of the rock.

3.2 | Numerical method

The deformation of rocks under compressive loads is solved using the balance equation for dynamics (Equation 8):

$$\rho_0 \ddot{\boldsymbol{\varphi}} = \nabla_{\boldsymbol{0}} \boldsymbol{\sigma_{PK}} + \rho_0 \boldsymbol{B}, \tag{8}$$

where $\boldsymbol{\varphi}$ is the displacement field, ρ_0 the initial density, $\boldsymbol{\sigma_{PK}}$ the first Piola-Kirchoff stress tensor, and $\boldsymbol{B}$ is the external applied force.

In this work, we solved the continuum problem using the penalty finite element formulation[29] by using our own simulator. Spatial discretization of the brazilian disc was performed with quadratic triangles. The time integration was implemented with a Newmark family predictor-corrector scheme.

To allow crack initiation and propagation in the rock model, a hybrid DG with a CZM was used.[29-32] This approach involves a generalization of the weak formulation of the continuum mechanics problem that allows for a solution of the displacement field that is discontinuous across the inter-element surfaces.

The DG-CZM has the advantage that the mesh topology does not need to be modified during the fracture process, and the consistency and stability of the uncracked inter-element surfaces are preserved.

Since the inter-element surfaces constitute the possible fracture paths, the method requires small elements' sizes to predict a representative fracture process.[33] Rigorous studies of the method's formulation are given in previous studies.[29-32]

It is important to highlight that the bulk elements are modeled using standard phenomenological material laws (VTI model in this case), while in the inter-element surfaces (cohesive elements), a phenomenological fracture indicator (fracture criterion) and a fracture energy release law as the one depicted in Figure 2 are used. Therefore, the effective linear irreversible cohesive model used here is considered extrinsic, since the CZM is only activated when a fracture criterion is achieved.

The specific constitutive behavior of cohesive elements after cohesive opening sets in is described by the relation between the cohesive traction $T = \boldsymbol{\sigma_{PK}} \cdot \boldsymbol{n}$, where $\boldsymbol{n}$ is the normal to the inter-element surface, and the opening

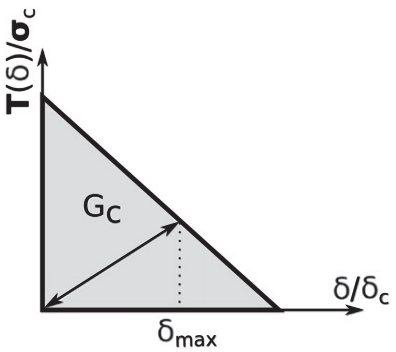

FIGURE 2 Effective linear irreversible cohesive law for a mode I fracture. The cohesive tractions T, impose the aperture length between elements; afterward, those tractions are a function of the crack opening displacement δ. σ_c is the critical strength of the rock material, and δ_c is the critical fracture opening before all the cohesion is lost. The area between the axes and the $T(\delta)$ curve is the material fracture energy G_c per unit volume

displacement $\delta = [\![\varphi]\!]$ across crack faces. These models were previously used for the simulation of dynamical problems,[34] fatigue,[35] and digital rock physics,[36] among others.

We show in Figure 2 the cohesive law for a mode I fracture. It is worth to mention that mode II fracture propagation is implemented in the same way as the mode I propagation. The cohesive tractions T impose the displacement continuity through inter-element surfaces; tractions are a function of the crack opening displacement as shown in Figure 2. In this figure, σ_c is the critical stress of the rock material and δ_c is the critical fracture opening before all cohesion is lost. In the same figure, the implemented model for an unloading/reloading process is shown. The area between the axes and the $T(\delta)$ curve is the material fracture energy G_c per unit volume.

In this model, it is assumed that the effective separation of the inter-element surfaces is given by

$$\delta = \sqrt{\gamma^2 \Delta_t^2 + \Delta_n^2}, \tag{9}$$

where Δ_t and Δ_n are the tangential and normal separation in the local deformed configurations, respectively. γ is a weight parameter for tangential separation.

As we stated before, the cohesive law is only activated when a fracture criterion is satisfied at the quadrature points of a cohesive element. A modified Mohr-Coulomb fracture criterion was used[33] as a fracture criterion in this work. Given a tensile stress in a quadrature point of a cohesive element, the fracture criterion is given by

$$\sqrt{\boldsymbol{\sigma_n}^2 + \left(\frac{\boldsymbol{\tau}}{\gamma}\right)^2} \geq \sigma_c. \tag{10}$$

On the other hand, for compression stresses, the fracture criterion is obtained as

$$|\boldsymbol{\sigma_n}| \geq |C_0 + tan(\phi)\boldsymbol{\tau}|, \tag{11}$$

where C_0 is the cohesion, ϕ the internal friction angle, and $\boldsymbol{\sigma_n}$ and $\boldsymbol{\tau}$ are the inter-element normal and tangential stress components.

Once the fracture criterion is satisfied, the cohesive element is activated, and the traction components in the inter-element surfaces are assumed to follow a linear relation.

$$\boldsymbol{T} = \frac{T}{\delta}(\gamma^2 \Delta_m \boldsymbol{m} + \Delta_n \boldsymbol{n}). \tag{12}$$

The traction-separation law ($T(\delta)$) shown in Figure 2 is given by

$$T(\delta, \delta_{max}) = \sigma_c \left(1 - \frac{\delta}{\delta_{max}}\right) \cdot \frac{ds}{dS} \quad for \quad \delta < \delta_c, \tag{13}$$

where ds/dS is the surface change between the reference and the deformed configuration. After a δ_c separation is reached, the element has null traction component, since it is completely detached.

3.3 | Brazilian test implementation

A transversely isotropic material was implemented to simulate the elastic and fracture response of laminated rocks. A 2D finite element mesh for the numerical simulation of the BT was generated. The meshes had about 3000 nonstructured elements and the BT disc model diameter was 50 mm for all the simulations. We show in Figure 3 a typical mesh with weak interfaces used in this work. The plane platens boundary conditions are also represented in this figure. An initial 10° contact angle is prescribed in the mesh. In all cases, the elements size is kept within the cohesive length required in CZM (see, for more details, Camacho and Ortiz[33]). It is important to note here that the use of nonstructured meshes with a proper elements size within the cohesive length have proven to mitigate mesh dependence in CZM, reducing this dependence both for crack initiation and propagation processes.[29]

The fracture initiation and propagation is assessed by a modified Mohr-Coulomb fracture criterion with an effective linear irreversible cohesive law. The effect of weak planes as interfaces of an anisotropic rock was studied varying the density and the fracture's properties of the planes.

Bulk elastic properties are shown in Table 1 and its fracture's properties in Table 2. Young modulus anisotropy used in our simulations for the matrix was 50% (horizontal to vertical). The Poisson ratio anisotropy was about 13.6%. All these values were in agreement with rock's properties found in the literature for a shale formation like Vaca Muerta, in the Neuquina Basin in Argentina (see, eg, Kosset[37] and Sosa Massaro et al[38]).

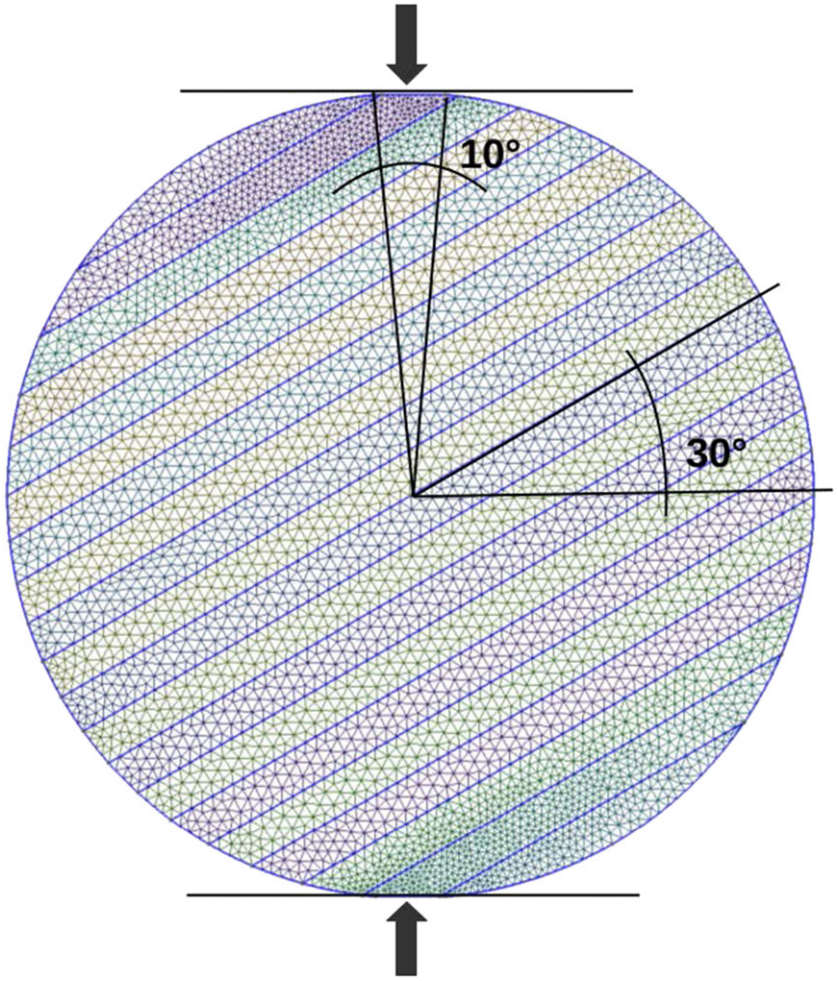

FIGURE 3 Finite element mesh with weak interfaces. The mesh has about 3000 nonstructured elements and 20 layers deviated 30° from the horizontal axis. The boundary condition has an initial contact angle of 10°, with plane platens moving at a constant displacement rate in compression mode [Colour figure can be viewed at wileyonlinelibrary.com]

TABLE 1 Vertically transversely isotropic elastic properties of the rock's matrix[a]

Parameter	Value	Unit
$E_h(\alpha = 0°)$	3.10×10^{10}	Pa
$E_v(\alpha = 90°)$	2.07×10^{10}	Pa
$\nu_h(\alpha = 0°)$	0.25	—
$\nu_v(\alpha = 90°)$	0.22	—
G_v	1.20×10^{10}	Pa

[a] E_h, ν_h, and E_v, ν_v are the Young modulus and Poisson ratio of the rock in horizontal and vertical directions, respectively. The anisotropy is 50% for the Young modulus. The Poisson ratio anisotropy is about 13.6%.

The effect of weak planes was taken into account as special discontinuities in the 2D disc model. These interfaces were modeled entirely as cohesive elements (ie, as a geometry in mesh elements without thickness and with only fracture's properties). The critical stress of the weak interfaces varied from 10% to 100% of that of the bulk, where the 100% represented the BT of an anisotropic rock without weak planes. Fracture properties of the interfaces used for the simulations are listed in Table 3.

TABLE 2 Fracture properties of the rock matrix[a]

Parameter	Value	Unit
σ_c	13.0×10^6	Pa
G_c	20	Pa·m
UCS	130×10^6	Pa
ϕ	38	°
C_0	3.2×10^6	Pa

[a] σ_c is the critical strength, G_c the material fracture energy per unit volume, UCS the unconfined strength, ϕ the internal friction angle, and C_0 the cohesion of the rock material.

TABLE 3 Fracture properties of the weak planes for different foliation-matrix's properties relations[a]

Parameter	10%	50%	100%	Unit
σ_c	$1.3E \times 10^6$	6.5×10^6	13.0×10^6	Pa
UCS	13.0×10^6	65.0×10^6	130×10^6	Pa
Φ	38	38	38	°
G_c	20	20	20	Pa·m
C_0	3.2×10^6	16.0×10^6	32.0×10^6	Pa
Layers	10/20/40	10/20/40	0	—
Spacing	5/2.5/1.25	5/2.5/1.25	0	mm

[a] 100% correspond to the model without weak interfaces. σ_c is the critical strength, G_c the material fracture energy per unit volume, UCS the unconfined strength, ϕ the internal friction angle, and C_0 the cohesion of the rock material. Spacing between 1.25 and 5 mm used in the models, produces 10, 20, and 40 total layers in the mesh, keeping the disc diameter constant.

The spacing of the planes was also varied. We ran simulations with 10, 20, and 40 layers keeping the disc diameter constant. We show the different spacings in Table 3.

The load was applied in the vertical direction with an average rate of 0.001 m/s (see Figure 3), while the isotropic plane angle (and the weak plane direction) was rotated from 0° to 90°. It is important to note that the direction of weak planes coincides with the isotropic plane of the matrix. The load velocity is faster than the standard experimental rates in order to avoid extensive computational time. Hasbani et al[39] showed that results of the simulations are not very sensitive to this rate.

Hertz contact conditions were implemented as boundary conditions for the loading. A contact angle of 10° was used with the purpose of avoiding states of stress concentrations and fracture's initiation near the point of the load's application.

The ultimate load was obtained in order to compute the BTS using both isotropic (Equation 1) and anisotropic expressions (Equation 2). The stress state in the whole model was analyzed during the loading and in the final prefracture condition in each simulation. Note that the associated error with the Claesson and Bohloli expression (Equation 2) is around 10% for the material's properties used in this study.

4 | RESULTS

Within this study, all simulations are two-dimensional, decreasing computation time and making the interpretation of results easier. This implies that all results are expressed per unit of thickness.

Force-displacement curves for the anisotropic BT without weak planes are shown in Figure 4 for different angles. As can be seen in this figure, there is a small variation in the ultimate load magnitude from 0° (lamination perpendicular to the applied load) to 90° (lamination parallel to the applied load) of rotation.

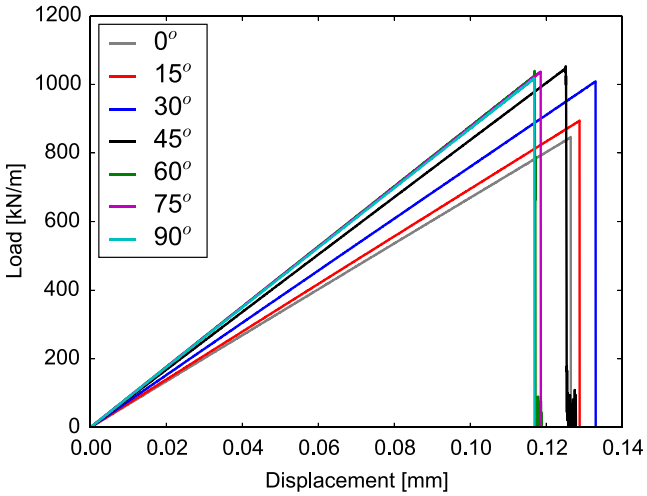

FIGURE 4 Force-displacement curves for vertically transversely isotropic rock without weak planes. Curves correspond to the BT with different foliation-loading angles. A variation in the ultimate load is shown from 0° to 90° of rotation due to the anisotropy of the rock's sample [Colour figure can be viewed at wileyonlinelibrary.com]

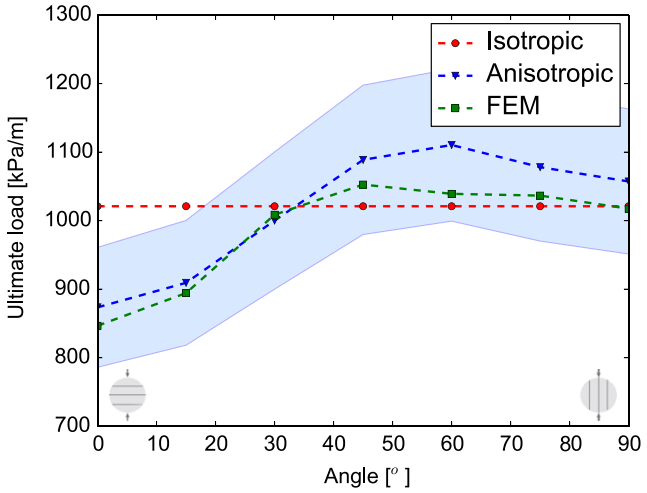

FIGURE 5 Anisotropic BT ultimate load as a function of the rotation angle. The dashed red line corresponds to the isotropic estimation of the ultimate load.[27] The dashed blue line corresponds to the Claesson and Bohloli approximate expression[15] and the dashed green line to the finite element solution of our simulations. The light blue area is the error in the approximate expression of Claesson and Bohloli[15] for the material properties used in this work [Colour figure can be viewed at wileyonlinelibrary.com]

The ultimate load is obtained using both Hondros' expression[27] and the Claesson and Bohloli's approximate expression[15] and compared with the ultimate load given by the finite element solution (Figure 4). The critical strength of the rock matrix (see Table 2) is used to obtain the ultimate load for the isotropic and the anisotropic material by applying Equations 1 and 2, respectively. The final load in all these simulations was obtained as the resultant load immediately before the crack's initiation.

Figure 5 shows the ultimate load of the BT without weak planes as a function of the rotation angle. The ultimate load has only a small variation with α, both in our finite element result (FEM) and in the approximate expression according to the critical strength of the BT. Although the isotropic prediction should not be valid for rocks with high anisotropy as those of our study, Hondros' expression remains within the error expected by the Claesson and Bohloli's approximate expression, except in the limit case in which the isotropic planes of the model are perpendicular to the applied load in the BT. As can be seen in Figure 5, the comparison of the Claesson and Bohloli's expression results with the numerical results is satisfactory.

The Mohr-Coulomb criterion for the homogeneous anisotropic rock is shown in Figure 6. Mohr circles were obtained with the principal stresses of our simulations at the BT disc's center and at the instant immediately before failing. As

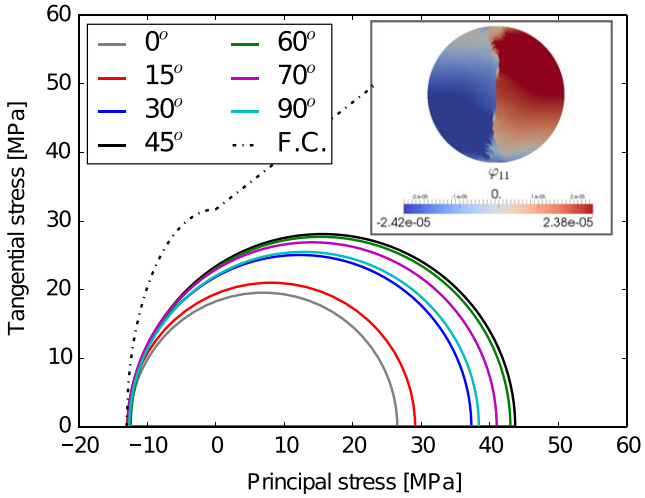

FIGURE 6 Mohr-Coulomb criterion for the anisotropic BT without weak planes as a function of the angle. The circles correspond to the principal stresses at the disc's center for different foliation-loading angles. In all cases, the fracture propagates in mode I, and the criterion is satisfied for a tensile stress state. The dashed black curve corresponds to the modified Mohr-Coulomb fracture criterion.[33] Inset: Fracture pattern for the anisotropic BT without weak planes and $\alpha = 15°$. The plot shows the displacement in the horizontal direction after the fracture propagates. The fracture initiates at the disc's center and propagates in the Y-direction (applied load direction) in mode I. Before reaching the edge of the disc, the stress concentration generated by the load application produces the branching of the fractures [Colour figure can be viewed at wileyonlinelibrary.com]

we expected, each angle has a different loading state that depends on the anisotropy of the material; and the fracture initiates in a tensile stress state in all cases. It is important to remark that the failure criterion used in all our simulations remains the same for the whole model and it does not vary with α, as shown in Table 2. Although the material's anisotropy influences the resulting stress state, the failure point occurs always at the same tensile value (σ_c).

Regarding the validity of using the tensile strength of anisotropic rock using the BT, the initiation of the fracture occurred at the disc's center, and the propagation was in the direction of the applied load in a mode I fracture, as expected. The inset of Figure 6 shows an example of the fracture pattern for these cases. As can be seen in the figure, the fracture initiates and propagates following the load direction in mode I until the fracture's tip reaches the stress concentration zone generated by the load application arc. Bifurcations of the main fracture are then observed.

4.1 | Anisotropic rock with weak interfaces

In this section, we consider weak interfaces aligned to the angle α. Figure 7 shows the typical load-displacement curves for the BT with weak interfaces. These results correspond to interfaces with the minimal value of critical strength of our simulations (10% of the matrix's strength; see Table 3). The spacing corresponds to the maximal density of weak interfaces in the model (40 layers in the whole sample). For this particular case, when the foliation-loading angle is between 0° and 30°, the loading curve deviates from the linear regime before achieving the ultimate load. This deviation is due to the matrix and interfaces being capable of supporting the load during the test. During the loading period, when a compressive critical stress is achieved in any interface, a sliding fracture process begins. However, the matrix is still able to support the increasing load. Finally, the fracture propagates abruptly in the loading direction. Taking into account that the critical strength of the interfaces is extremely low in comparison with that of the matrix (10%), for high orientation angles (over 45°), the fracture initiates and propagates entirely through the weak planes.

Figure 8 shows the failure criteria and the Mohr circles obtained for our simulations of the BT with weak planes (WP) that have a critical strength of 50% of the matrix's strength and 10 layers in the model (5-mm spacing). These Mohr circles were obtained using the principal stresses at the disc's center at the moment immediately before fracture nucleation. In these circles, solid lines correspond to the stress state in the rock's matrix, whereas the marked points on the circle circumference correspond to the stress state in the weak plane. These points can be decomposed in shear and normal stress components acting on the weak interface.

Notice that, in order to evaluate the fracture nucleation in the heterogeneous anisotropic specimen, the stress state of the matrix should be compared with the matrix's failure criterion (FC) and, accordingly, the WP stress state with its

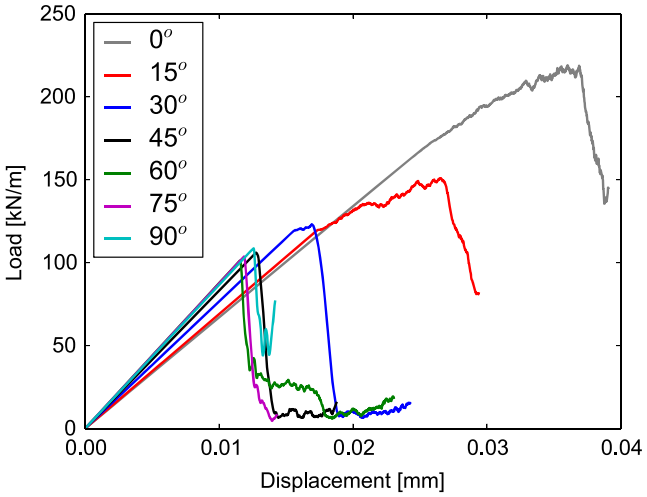

FIGURE 7 Load-displacement curves for the BT with weak interfaces. These results correspond to planes with a critical stress of 10% of the matrix's strength ($\sigma_c = 1.3E \times 10^6$) and the maximal density of weak interfaces (40 layers in the whole model) with a spacing of 1.25 mm [Colour figure can be viewed at wileyonlinelibrary.com]

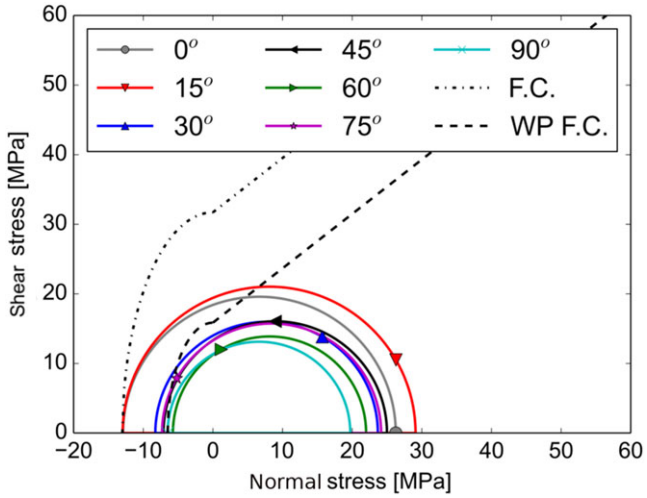

FIGURE 8 Failure criteria and Mohr circles for the BT with weak interfaces. The results correspond to a critical strength for the interfaces $\sigma_c = 6.5 \times 10^6$ Pa (50% of the matrix's strength) and a 5-mm spacing between planes (10 layers in the whole sample). The stress states were taken at the center of the disc [Colour figure can be viewed at wileyonlinelibrary.com]

failure criterion (WP FC). The stress state at the center of the specimen generates a tensile failure of the rock matrix for 0° and 15°, and a tensile failure of the weak interfaces for 75° and 90°. However, for the orientations in between (30°, 45°, and 60°), the given stress states at the center satisfy neither the matrix's nor the weak interface's failure criteria, and consequently, fracture nucleation does not occur at the specimen center at the moment of fracture initiation. This behavior is different from the one found in homogeneous anisotropic rocks shown in Figure 6, where fractures were nucleated at the specimen's center for all orientations.

Brazilian tests with fracture initiation outside the center are common for foliated anisotropic rocks.[7,8] Anisotropic elastic properties generated by finely stratified sedimentary rocks, and the presence of well-defined planes acting as interfaces, produce this type of phenomenon, mainly due to the lower strength of the laminations.

The suggested ISRM method[5] for tensile strength characterization requires a 10° contact loading angle for the isotropic analytical expression to be valid. Some studies have already demonstrated (see, eg, Erarslan and Williams[18]) that higher contact angles with an elliptical loading jaw should be used in order to initiate the fracture at the disc center.

With the elastic properties and contact angle considered, we found that the fracture initiates outside the disc center for some foliation orientations. Since the commonly used expressions to obtain the brazilian test strength consider a centered failure initiation, the out-of-center failure underestimates the strength of the sample.

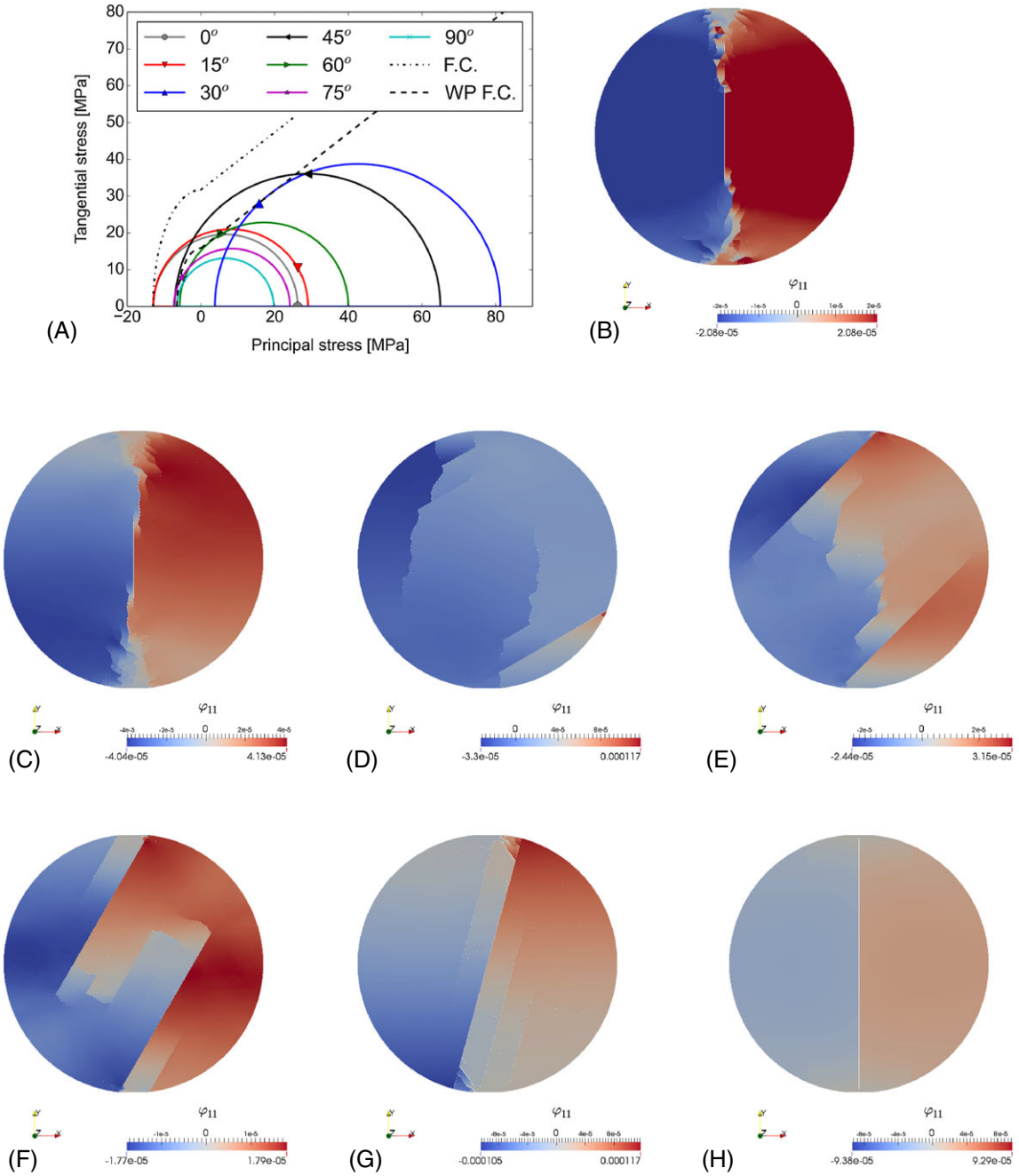

FIGURE 9 (A) Failure criteria and Mohr circles for the BT with weak interfaces. The results correspond to a critical strength for the interfaces $\sigma_c = 6.5 \times 10^6$ Pa (50% of the matrix's strength) and a 5-mm spacing between interfaces (10 layers in the whole sample). The stress states were taken at the position of fracture nucleation. (B) The plot corresponds to the fracture pattern for an orientation angle $\alpha = 0°$. The color map represents the displacement in the X-direction of the rock after fracture propagation. (C) For $\alpha = 15°$. (D) For $\alpha = 30°$. (E) For $\alpha = 45°$. (F) For $\alpha = 60°$. (G) For $\alpha = 75°$. (H) For $\alpha = 90°$ [Colour figure can be viewed at wileyonlinelibrary.com]

In Figure 9A, we plot Mohr circles taking the stress state at the points of fracture nucleation for the same simulations of Figure 8. As mentioned before, the stress state in the matrix is given by the solid circle, and it is compared with the matrix failure criterion; the marked point represents the stress state in the interface, and it is compared with the weak plane failure criterion. When using the nucleation points to extract the stress states, rather than the disc's center, one of the two failure criteria is satisfied for all the orientations.

Two failure mechanisms are recognized in Figure 9A: a pure tensile failure and a mixed mode, which has a sliding failure component. For low orientation angles, where the load is applied nearly perpendicular to the foliation plane, the

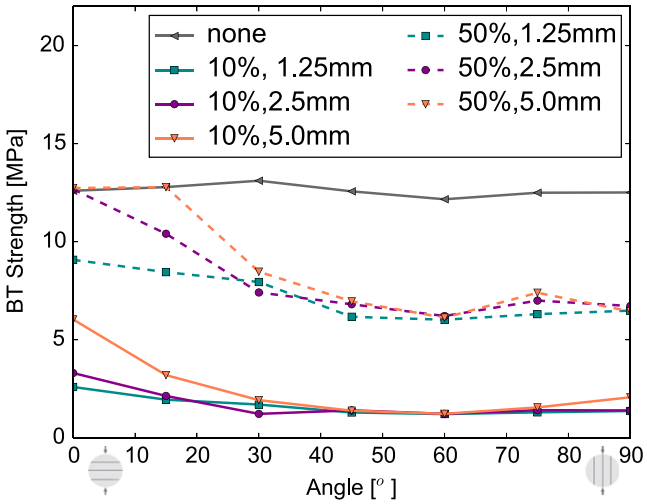

FIGURE 10 Effect of the critical strength and density of weak interfaces on the BT's strength as a function of the foliation-loading angle. The dark gray line corresponds to the BT without weak interfaces as a reference. The orange, purple, and green lines correspond to $\sigma_c = 1.3E \times 10^6$ and 10, 20, and 40 layers, respectively. The dashed orange, purple, and green lines correspond to $\sigma_c = 6.5 \times 10^6$ and 10, 20, and 40 layers, respectively [Colour figure can be viewed at wileyonlinelibrary.com]

stress state in the loading axis generates the fracture initiation at the disc's center and the propagation crossing the rock's matrix. Fracture patterns are shown in Figure 9B,C for 0° and 15°, respectively.

For intermediate angles (30°, 45°, 60°, and 75°), we found sliding failure across the weak interfaces. The critical stress state in the weak plane has a shear stress component at the moment of the fracture nucleation. Typical fracture patterns obtained for each of these orientation angles are shown in Figure 9D-G for 30°, 45°, 60°, and 75°, respectively. For 90°, where the foliation planes are parallel to the loading direction, the fracture initiates and propagates along a weak plane in a tensile mode. In Figure 9H, we plot the fracture pattern for this simulation.

Finally, we summarize the effect of the critical strength, cohesion, and density of weak interfaces on the strength of the disc in Figure 10. The fracture's properties used for these simulations are listed in Table 3. The BT's strength was obtained as the resultant tensile stress by finite elements at the nucleation point of the first generated fracture on the loading axis, immediately before the crack's initiation.

Although the interface's density does not have a pronounced effect on the BT's strength under the conditions of this work, the disc's strength is strongly affected by the fracture's properties of the planes. As can be seen in Figure 10, the strength varies with the foliation-loading angle. While the strength remains practically constant for the discs without interfaces, by including the planes, the disc's strength strongly decreases.

As expected, when the interfaces are close to being parallel to the load's application direction ($\alpha \simeq 90°$), BT's strength corresponds to the strength of the interface, given that the fracture initiates and propagates through it. We also found that the interface's density only affects BT's strength for low angles. The greater the number of interfaces, the faster the decrease of the strength while the foliation-loading angle increases. The number of interfaces modifies the stress distribution in the disc, generating a reduction in the final strength of the rock.

Notice that we do not discuss the results as “tensile strength of the rock” but rather as the “BT's strength” in a general manner. For the cases without weak planes, the anisotropy only modifies the stress state on the disc, but finally, a tensile stress (greater than the rock's critical stress σ_c) is obtained at the disc's center that produces the tensile failure. When weak planes are present, fractures do not always occur in mode I, and the obtained tensile strength is no longer valid.

The use of the BT to characterize highly foliated rocks has some undesired consequences. For laminated rocks with low cohesion cement or foliated rocks with low strength mineral alignment, the BT will mainly estimate the strength of weak planes. On the other hand, for rocks with stronger interfaces (50% of the matrix strength), the spacing of the interfaces will affect the BT strength estimation. It should be stated that for a spacing of 1.25 mm of interfaces with 50% of the matrix's strength, the fracture initiation and propagation occurs near the loading jaws. To prevent this, a higher contact angle should be used as proposed by Erarslan et al.[18] This would mean deviating from the ISRM suggested method,[5] and a new expression for BT strength should be used if a higher loading contact angle is used.

As a final comment, it should be noted that the sliding failure process used in this model consists of two sliding surfaces with no friction between them. It remains for future work to incorporate a friction law for sliding broken inter-elements.

5 | CONCLUSIONS

In this work, the effect of weak interfaces in the fracture behavior of vertically transversely isotropic rocks was assessed numerically. A model that incorporates an anisotropic elastic constitutive law with a discrete set of weak interfaces parallel to the isotropic direction was implemented. We varied the fracture's critical strength, the cohesion, and the density of the weak interfaces in the model.

In general, the finite element results are well captured by the anisotropic estimation of the BT ultimate load given by Claesson and Bohloli[15] for rocks without weak interfaces. Given the anisotropic relation $E_h/E_v = 1.5$ used in this work, the numerical results obtained are within the 10% estimated error for that anisotropic expression. If the isotropic expression[27] were used for anisotropic rocks, the stress state at the center of the sample would be underestimated.

The presence of weak planes affects the fracture nucleation and propagation. Different fracture modes were obtained, namely, tensile failure across the rock's matrix, shear sliding of weak planes, and tensile failure across them. It should be mentioned here that the fracture patterns obtained numerically in this work are consistent with the ones found experimentally in literature for anisotropic rocks.[8]

For low critical strength of the weak planes, both loading direction and interface's density have a small effect on the BT strength, since the fracture behavior is fully governed by the low strength of the interfaces.

For intermediate values of the critical strength, the matrix anisotropy becomes relevant in the fracture process. For low orientation angles, the interfaces spacing has a strong effect on the BT strength. For low density (high spacing), the matrix strength governs the fracture process. For high loading angles, the fracture process is governed by the weak plane's strength. We found that for some intermediate angles, the fracture begins outside of the center of the specimens. Stress states shown in the Mohr circles can explain the failure mechanisms. A detailed analysis between the stress states on the weak interfaces and the out-of-center fracture initiation in the brazilian test (knowing the distribution of tensions on the disc) could be a starting point for experimentally estimating the mechanical properties of the weak planes.

The characterization of the fracture properties of the interfaces in anisotropic rocks should be a rigorous process in order to determine their effect on rock strength.

ACKNOWLEDGEMENTS

The authors thank YPF-Tecnología S.A. for the permission to publish this article and financial support. H.M.C. and J.L.O. acknowledge the support of CONICET (Argentina). The authors also thank E. Winograd (YPF-Tecnología S.A.) for the technical contribution. H.M.C. acknowledges the support and help of Professor R. Radovitzky (Massachusetts Institute of Technology).

ORCID

Humberto M. Celleri http://orcid.org/0000-0002-1964-8144

REFERENCES

1. Mavko G, Mukerji T, Dvorkin J. *The Rock Physics Handbook: Tools for Seismic Analysis of Porous Media*. Cambridge: Cambridge Press; 2009.
2. Ouchterlony F. Fracture toughness testing of rock with core based specimens. *Eng Frac Mech*. 1990;35(1/2/3):351-366.
3. Kuruppu MD, Obara Y, Ayatollahi MR, Chong KP, Funatsu T. ISRM—suggested method for determining the mode I static fracture toughness using semi-circular bend specimen. *Rock Mech Rock Eng*. 2014;47:267-274.
4. Fowell RJ, Xu C. The cracked chevron notched brazilian disc test: geometrical considerations for practical rock fracture toughness measurement. *Int J Rock Mech Min Sci*. 1993;30(7):821-824.
5. Bieniawski ZT, Hawkes I. ISRM—suggested methods for determining tensile strength of rock materials. *Int J Rock Mech Min Sci*. 1978;15:99-103.
6. Vervoort A, Min KB, Konietzky H, et al. Failure of transversely isotropic rock under brazilian test conditions. *Int J Rock Mech Min Sci*. 2014;70:343-352.

7. Debecker B, Vervoort A. Experimental observation of fracture patterns in layered slate. *Int J Fracture*. 2009;159(1):51-62.
8. Tavallali A, Vervoort A. Effect of layer orientation on the failure of layered sandstone under brazilian test conditions. *Int J Rock Mech Min Sci*. 2010;47(2):313-322.
9. Tavallali A, Vervoort A. Failure of layered sandstone under brazilian test conditions: effect of micro-scale parameters on macro-scale behaviour. *Rock Mech Rock Eng*. 2010;43:641-653.
10. Tan X, Konietzky H, Frühwirt T, Dan DQ. Brazilian tests on transversely isotropic rocks: laboratory testing and numerical simulations. *Rock Mech Rock Eng*. 2015;48:1341-1351.
11. Khanlari G, Rafiei B, Abdilor Y. An experimental investigation of the brazilian tensile strength and failure patterns of laminated sandstones. *Rock Mech and Rock Eng*. 2015;48(2):843-852.
12. Mighani S, Sondergeld CH, Rai CS. Observations of tensile fracturing of anisotropic rocks. *Soc Petrol Eng J*. 2016;21:1-13.
13. Amadei B, Rogers JD, Goodman RE. Elastic constants and tensile strength of anisotropic rocks. *Int Cong Rock Mech*. 1983;189-196.
14. Chen C, Pan E, Amadei B. Determination of deformability and tensile strength of anisotropic rock using brazilian tests. *Int J Rock Mech Min Sci*. 1998;35(1):43-61.
15. Claesson J, Bohloli B. Brazilian test: stress field and tensile strength of anisotropic rocks using an analytical solution. *Int J Rock Mech Min Sci*. 2002;39(8):991-1004.
16. Cho J, Kim H, Jeon S, Min KB. Deformation and strength anisotropy of Asan gneiss, Boryeong shale, and Yeoncheon schist. *Int J Rock Mech Min Sci*. 2012;50:158-169.
17. Kourkoulis SK, Markides CF, Chatzistergos PE. The standardized brazilian disc test as a contact problem. *Int J Rock Mech Min Sci*. 2013;57:132-141.
18. Erarslan N, Williams DJ. Experimental, numerical and analytical studies on tensile strength of rocks. *Int J Rock Mech Min Sci*. 2012;49:21-30.
19. Debecker B, Vervoort A. Two-dimensional discrete element simulations of the fracture behaviour of slate. *Int J Rock Mech Min Sci*. 2013;61:161-170.
20. Yang SQ, Huang YH. Particle flow study on strength and meso-mechanism of brazilian splitting test for jointed rock mass. *Acta Mech Sinica*. 2014;30(4):547-558.
21. Park B, Min KB. Bonded-particle discrete element modeling of mechanical behavior of transversely isotropic rock. *Int J Rock Mech Min Sci*. 2015;76:243-255.
22. Duan K, Kwok CY, Pierce M. Discrete element method modeling of inherently anisotropic rocks under uniaxial compression loading. *Int J Numer Anal Met*. 2016;40(8):1150-1183.
23. Mahabadi OK, Randall NX, Zong Z, Grasselli G. A novel approach for micro-scale characterization and modeling of geomaterials incorporating actual material heterogeneity. *Geophys Res Lett*. 2012;39:L01303. ISSN: 1944-8007.
24. Guo L, Latham J, Xiang J. A numerical study of fracture spacing and through-going fracture formation in layered rocks. *Int J Solids Struct*. 2017;110:44-57.
25. Mahjoub M, Rouabhi A, Tijani M, Granet S. An approach to model the mechanical behavior of transversely isotropic materials. *Int J Numer Anal Met*. 2016;40(6):942-961.
26. Li D, Liu G, Wong LNY. The Brazilian disc test for rock mechanics application: review and new inside. *Rock Mech Rock Eng*. 2013;46:107-121.
27. Hondros G. The evaluation of Poisson's ratio and the modulus of materials of a low tensile resistance by the brazilian (indirect tensile) test with particular reference to concrete. *Aust J App Sci*. 1959;10:243-268.
28. Suarez-Rivera R, Deenadayalu C, Chertov M, Hartanto RN, Gathogo P, Kunjir R. Improving horizontal completions on heterogeneous tight shales. *Soc Petrol Eng J*. 2011.
29. Radovitzky R, Seagraves A, Tupek M, Noels L. A scalable 3D fracture and fragmentation algorithm based on a hybrid, discontinuous Galekin, cohesive element method. *Comput Method Appl M*. 2011;200:326-344.
30. Noels L, Radovitzky R. A general discontinuous Galerkin method for finite hyperelasticity. Formulation and numerical applications. *Int J Numer Meth Eng*. 2006;68(1):64-97.
31. Noels L, Radovitzky R. Alternative approaches for the derivation of discontinuous Galerkin methods for nonlinear mechanics. *J Appl Mech*. 2007;74:1031-1036.
32. Noels L, Radovitzky R. An explicit discontinuous Galerkin method for nonlinear solid mechanics: formulation, parallel implementation and stability properties. *Int J Numer Meth Eng*. 2008;74:1393-1420.
33. Camacho GT, Ortiz M. Computational modelling of impact damage in brittle materials. *Int J Solids Struct*. 1996;33(20): 2899-2938.
34. Ortiz M, Pandolfi A. Finite-deformation irreversible cohesive elements for three-dimensional crack-propagation analysis. *Int J Numer Meth Eng*. 1999;44(9):1267-1282.
35. Nguyen O, Repetto EA, Ortiz M, Radovitzky RA. A cohesive model of fatigue crack growth. *Int J Fracture*. 2001;110(4):351-369.
36. Winograd EA, Bosco S, Álvarez JP, Mendoza M, Hryb D, Sánchez M. Characterization of mechanical properties of rocks using numerical simulation and image analysis. In: Proceedings of the 49th U.S. Rock Mechanics/Geomechanics Symposium; 2015; San Francisco, California.

37. Kosset T. *Wellbore Integrity Analysis for Wellpath Optimization and Drilling Risks Reduction: The Vaca Muerta Formation*. Colorado, USA: PhD Dissertation, Colorado School of Mines; 2014.

38. Sosa Massaro A, Espinoza DN, Frydman M, Barredo S, Cuervo S. Analyzing a suitable elastic geomechanical model for Vaca Muerta formation. *J S Am Earth Sci*. 2017;79(Supplement C):472-488.

39. Hasbani J, Sánchez M, Rosolen A, et al. On the computational modeling of hydraulic fracturing processes. In: Proceedings of the 9th Hydrocarbon Exploration and Development Congress and Exhibition; 2014; Mendoza, Argentina.

How to cite this article: Celleri HM, Sánchez M, Otegui JL. Fracture behavior of transversely isotropic rocks with discrete weak interfaces. *Int J Numer Anal Methods Geomech*. 2018;1–16. https://doi.org/10.1002/nag.2849